The m^{6}A reader protein YTHDC2 interacts with the small ribosomal subunit and the 5′–3′ exoribonuclease XRN1

JENS KRETSCHMER,[1] HARITA RAO,[2] PHILIPP HACKERT,[1] KATHERINE E. SLOAN,[1] CLAUDIA HÖBARTNER,[2,3] and MARKUS T. BOHNSACK[1,4]

[1]Department of Molecular Biology, University Medical Centre Göttingen, 37073 Göttingen, Germany
[2]Institute for Organic and Biomolecular Chemistry, Georg-August-University, 37077 Göttingen, Germany
[3]Institute for Organic Chemistry, University Würzburg, 97074 Würzburg, Germany
[4]Göttingen Center for Molecular Biosciences, Georg-August-University, 37073 Göttingen, Germany

ABSTRACT

N^6-methyladenosine (m^{6}A) modifications in RNAs play important roles in regulating many different aspects of gene expression. While m^{6}As can have direct effects on the structure, maturation, or translation of mRNAs, such modifications can also influence the fate of RNAs via proteins termed "readers" that specifically recognize and bind modified nucleotides. Several YTH domain-containing proteins have been identified as m^{6}A readers that regulate the splicing, translation, or stability of specific mRNAs. In contrast to the other YTH domain-containing proteins, YTHDC2 has several defined domains and here, we have analyzed the contribution of these domains to the RNA and protein interactions of YTHDC2. The YTH domain of YTHDC2 preferentially binds m^{6}A-containing RNAs via a conserved hydrophobic pocket, whereas the ankyrin repeats mediate an RNA-independent interaction with the 5′–3′ exoribonuclease XRN1. We show that the YTH and R3H domains contribute to the binding of YTHDC2 to cellular RNAs, and using crosslinking and analysis of cDNA (CRAC), we reveal that YTHDC2 interacts with the small ribosomal subunit in close proximity to the mRNA entry/exit sites. YTHDC2 was recently found to promote a "fast-track" expression program for specific mRNAs, and our data suggest that YTHDC2 accomplishes this by recruitment of the RNA degradation machinery to regulate the stability of m^{6}A-containing mRNAs and by utilizing its distinct RNA-binding domains to bridge interactions between m^{6}A-containing mRNAs and the ribosomes to facilitate their efficient translation.

Keywords: RNA modification; N^6-methyladenosine (m^{6}A); YTH domain; ribosome; translation; exoribonuclease

INTRODUCTION

RNA modifications in diverse cellular RNAs, often collectively termed the "epitranscriptome," have emerged as important regulators of most aspects of gene expression (Roundtree et al. 2017a). The presence of N^6-methyladenosine (m^{6}A) in mRNAs was first detected several decades ago (see for example, Desrosiers et al. 1974; Adams and Cory 1975; Dubin and Taylor 1975). However, the recent development of approaches for the transcriptome-wide mapping of m^{6}A sites has enabled the functional importance of these modifications to be explored as they have provided inventories of m^{6}A-modified transcripts and defined the positions of m^{6}A modifications within these RNAs (Dominissini et al. 2012; Meyer et al. 2012; Chen et al. 2015; Linder et al. 2015). So far, in excess of 10,000 m^{6}A sites have been reported and approximately one in four mRNAs are suggested to carry such modifications (Xuan et al. 2017). While m^{6}A modifications have been detected in both 5′ and 3′ untranslated regions (UTRs) as well as introns and exons, they are typically enriched in 3′ UTRs in close proximity to stop codons and have often been observed to form clusters (Meyer et al. 2012). The majority of m^{6}A modifications lie within a DRACH motif (D = A, G or U; R = A or G; H = A, C or U) and are thought to be introduced cotranscriptionally by a methyltransferase complex composed of METTL3, METTL14, WTAP, RBM15/RBM15B, and KIAA1429 (Liu et al. 2014; Ping et al. 2014; Schwartz et al. 2014; Patil et al. 2016; Ke et al. 2017). Structural and functional studies have shown that METTL3 is an active, *S*-adenosylmethionine-dependent m^{6}A methyltransferase while METTL14 acts as an RNA-binding platform that, together

Corresponding author: markus.bohnsack@med.uni-goettingen.de
Article is online at http://www.rnajournal.org/cgi/doi/10.1261/rna.064238.117. Freely available online through the *RNA* Open Access option.

with RBM15/RBM15B, plays an important role in substrate recognition and binding (Patil et al. 2016; Wang et al. 2016a,b). WTAP is suggested to serve as a structural scaffold that regulates the localization and catalytic activity of the complex (Ping et al. 2014). Recently, METTL16 was identified as a second active m^{6}A methyltransferase in human cells that is responsible for N^6-methylation of the U6 snRNA and the MAT2A mRNA, which both contain m^{6}A modifications in non-DRACH sequence contexts (Pendleton et al. 2017; Warda et al. 2017).

Interestingly, many m^{6}A modifications have been reported to be sub-stoichiometric, suggesting that they are installed dynamically (Dominissini et al. 2012; Meyer et al. 2012; Meyer and Jaffrey 2017). The concept of dynamic m^{6}A modification was expanded by the discovery that ALKBH5 and FTO can act as demethylases (Jia et al. 2011; Zheng et al. 2013), implying that m^{6}A modifications are reversible. More recently however, FTO was suggested to preferentially demethylate m^{6}Am modifications present at the cap+1 and cap+2 positions of many mRNAs (Mauer et al. 2017), and upon release of nascent RNA transcripts from chromatin, m^{6}As were found to be relatively stable (Ke et al. 2017). Such regulation of m^{6}A modifications in mRNAs has been suggested to play important roles in regulating alternative splicing and 3′ end mRNA processing (Bartosovic et al. 2017) as well as in stress responses (Schwartz et al. 2013; Zhou et al. 2015). Furthermore, alterations in the levels and sites of m^{6}A modification are implicated in modulating gene expression during development (Lence et al. 2016; Zhao et al. 2017a; Yu et al. 2018), differentiation (Xu et al. 2017), and tumorigenesis (Cui et al. 2017).

The presence of m^{6}A modifications can directly influence cellular RNAs by altering their secondary structure and/or interactions with RNA-binding proteins (Liu et al. 2015; Roost et al. 2015). Similarly, m^{6}A modifications can determine the translational dynamics of mRNAs by affecting codon–anticodon base-pairing with tRNAs in the ribosome (Choi et al. 2016) and have been shown to influence the utilization of alternative polyadenylation sites (Ke et al. 2015; Molinie et al. 2016). Alternatively, m^{6}A modifications can influence the fate of RNAs via proteins (termed "readers") that specifically recognize and bind modified nucleotides. Several such m^{6}A reader proteins have been identified, many of which contain a YTH domain (Zhang et al. 2010; Wang and He 2014). The core of the YTH domain is composed of a six-stranded β-sheet surrounded by three α-helices, which form a positively charged surface and a deep hydrophobic pocket that mediates interactions with the m^{6}A (Theler et al. 2014). Interestingly, it was recently suggested that the YTH domains of YTHDF1-3 can also specifically recognize N^1-methyladenosine (m^{1}A) modifications in cellular RNAs via their hydrophobic pocket (Dai et al. 2018). In the nucleus, YTHDC1 binds specific m^{6}A-containing pre-mRNAs and regulates their splicing by promoting recruitment of the splicing factor SRSF3 and impeding their interactions with SRSF10 (Xiao et al. 2016). Similarly, a non-YTH domain-containing reader protein HNRNPA2B1 binds m^{6}A-containing pre-mRNAs and regulates their alternative splicing (Alarcón et al. 2015). In addition to their functions in splicing regulation, HNRNPA2B1 associates with m^{6}A-methylated primary microRNAs to promote their processing (Alarcón et al. 2015), and YTHDC1 binds m^{6}A residues in the long noncoding RNA XIST regulating its function in transcriptional silencing of X-chromosome genes (Patil et al. 2016) as well as influencing use of alternative polyadenylation sites (Kasowitz et al. 2018) and mediating the nuclear export of selected m^{6}A-containing pre-mRNAs (Roundtree et al. 2017b). In the cytoplasm, YTHDF1 enhances the translation of m^{6}A-modified mRNAs by bridging interactions with translation initiation factors, thereby facilitating highly efficient cap-dependent translation (Wang et al. 2015). Interestingly, METTL3 was shown to have a methyltransferase-independent function as an m^{6}A reader that associates with ribosomes and promotes translation of a subset of m^{6}A-containing mRNAs by facilitating recruitment of eIF3 during translation initiation (Lin et al. 2016). Similarly, insulin-like growth factor 2 mRNA-binding proteins (IGF2BP1/2/3) were recently identified as non-YTH m^{6}A reader proteins that promote mRNA stability and translation (Huang et al. 2018). In contrast, the binding of YTHDF2 to m^{6}A-containing mRNAs causes their relocalization to processing bodies and accelerates their degradation by recruiting the CCR4-NOT deadenylation complex (Wang et al. 2014; Du et al. 2016). Finally, YTHDF3 was found to share many common target mRNAs with YTHDF1 and YTHDF2, and has been suggested to function cooperatively with these proteins to enhance translation and decay of these mRNAs (Shi et al. 2017). Taken together, these findings have led to the proposal that m^{6}A modifications in mRNAs act as markers that direct particular transcripts for accelerated processing, translation, and decay, enabling rapid and short-lived alterations in the expression of specific genes under certain conditions or during particular growth phases (e.g., development or cell differentiation). It is suggested that m^{6}A methylation represents a means by which the expression of a myriad of mRNAs that encode proteins required for a given cellular process, but that have diverse properties (stabilities, translation efficiencies, etc.), can be efficiently coordinated (Zhao et al. 2017b).

The fifth YTH domain-containing protein in human cells, YTHDC2, differs from the other family members as, in addition to its YTH domain, it contains other putative RNA-binding domains. Here, we analyze the contribution of different domains of YTHDC2 to its functions and show that the YTH domain preferentially binds m^{6}A-containing RNAs and that both the YTH and R3H domains contribute the binding of YTHDC2 to cellular RNAs. We further demonstrate that the ankyrin repeats within the

helicase core of YTHDC2 mediate an interaction with the 5′–3′ exoribonuclease XRN1, suggesting that YTHDC2 may play a role in regulating mRNA stability. Our data reveal an interaction of YTHDC2 with ribosomes and using in vivo crosslinking, we identify a YTHDC2 binding site on the small ribosomal subunit in close proximity to the mRNA entry site, suggesting that YTHDC2 may facilitate the efficient translation of specific m^{6}A-containing mRNAs by bridging interactions with the ribosome.

RESULTS

The YTH domain of YTHDC2 preferentially associates with m^{6}A-containing RNAs via a conserved hydrophobic m^{6}A-binding pocket

Among the five human YTH domain-containing proteins, YTHDC2 is unique as it contains several annotated domains in addition to the common YTH domain, namely, an R3H domain and a DEAH-box helicase core domain punctuated by two ankyrin repeats (Fig. 1A). We therefore first set out to determine the key interactions formed by each of these regions of the protein. YTH domains have been shown to specifically bind RNAs that contain m^{6}A modifications enabling YTH domain-containing proteins to act as modification readers and regulate the fate of m^{6}A-containing RNAs. To demonstrate that the YTH domain of YTHDC2 also specifically recognizes m^{6}A-modified RNAs, we performed in vitro anisotropy experiments to determine the affinity of the YTH domain of YTHDC2 (amino acids 1277–1430) for unmodified and m^{6}A-containing RNAs. Transcriptome-wide identification of m^{6}A sites has revealed that the majority of these modifications lie within a DRACH motif, with GGACU being the most commonly observed sequence context. Therefore, fluorescently labeled, 9-nucleotide RNAs containing a GGACU sequence in which the adenosine was either unmodified or substituted for an N^6-methyladenosine were synthesized (Fig. 1B). Furthermore, the YTH domain of YTHDC2 was recombinantly expressed in *E. coli* with an N-terminal His_6-ZZ tag and purified (Fig. 1C), then increasing amounts of protein were incubated with the fluorescein-labeled RNAs. While almost no binding of the YTH domain of YTHDC2 (YTH) to the RNA containing an unmodified GGACU sequence was observed, YTH bound to the GGm^{6}ACU-containing RNA with a K_d of 3.2 ± 0.3 μM (Fig. 1D), demonstrating that the YTH domain of YTHDC2 has significantly higher affinity for m^{6}A-containing than unmodified RNAs.

Structural analysis of the YTH domain of YTHDC1 bound to an m^{6}A nucleoside demonstrated that the modified residue is encased in a hydrophobic pocket formed by aromatic tryptophan residues (W377 and W428; Xu et al. 2014). Alignment of the amino acid sequences of the five human YTH domains using MAFFT (Robert and Gouet 2014) revealed that these residues are conserved in YTHDC2 (Fig. 1E). Therefore, to determine if these residues also contribute to m^{6}A-recognition by the YTH domain of YTHDC2, we expressed the YTH domain of YTHDC2 in which W1310 or W1360 were converted to alanine (Fig. 1C). In contrast to the wild-type YTH domain of YTHDC2, these mutants did not stably associate with GGm^{6}ACU-containing RNAs (Fig. 1F), demonstrating that the mechanism of m^{6}A-binding by YTHDC2 is similar to that of other YTH domain-containing proteins.

The R3H and YTH domains contribute to the binding of YTHDC2 to cellular RNAs

The binding of the YTH domain of YTHDC2 to m^{6}A-containing RNAs in vitro implies that it likely participates in the association of YTHDC2 with cellular RNAs, but YTHDC2 also contains another putative RNA-binding domain, the R3H domain (Fig. 1A). Therefore, to analyze the contribution of these two domains to the binding of YTHDC2 to cellular RNAs, HEK293 cell lines for the expression of His_6-PreScission protease cleavage site-2x Flag (Flag)-tagged full-length YTHDC2 (YTHDC2-Flag) or Flag-tagged forms of YTHDC2 lacking either the R3H domain (ΔR3H-Flag) or the YTH domain (ΔYTH-Flag) were generated. Cells expressing the full-length or truncated proteins to equal levels (Fig. 2A, lower panel) were grown in the presence of 4-thiouridine before crosslinking using light of 365 nm. Covalently linked protein–RNA complexes were retrieved by tandem affinity purification under native and denaturing conditions. RNAs copurified with YTHDC2 were radiolabeled at the 5′ end using [^{32}P], complexes were separated by denaturing polyacrylamide gel electrophoresis, transferred to a nitrocellulose membrane, and RNAs were visualized by autoradiography (Fig. 2A, upper panel). While full-length YTHDC2 was efficiently crosslinked to cellular RNAs, the amounts of RNA retrieved when either the YTH domain or the R3H domain were lacking were notably reduced. These data demonstrate that both the YTH and R3H domains contribute to the in vivo RNA binding and cellular function of YTHDC2.

YTHDC2 associates with the 5′–3′ exoribonuclease XRN1 via its ankyrin repeat domains

In contrast to the RNA-binding YTH and R3H domains, ankyrin repeats are typically involved in mediating protein–protein interactions. Therefore, to gain insight into the protein interaction network of YTHDC2 and the potential role of its ankyrin repeats, protein interaction partners of YTHDC2 were identified by immunoprecipitation experiments (IP) from HEK293 cells expressing either N- or C-terminally Flag-tagged YTHDC2, or the Flag tag, and analysis of the eluates by mass spectrometry. Proteins that were more than 2.5 $\log_2$ fold enriched in the eluates of both YTHDC2 IPs compared to the control sample were

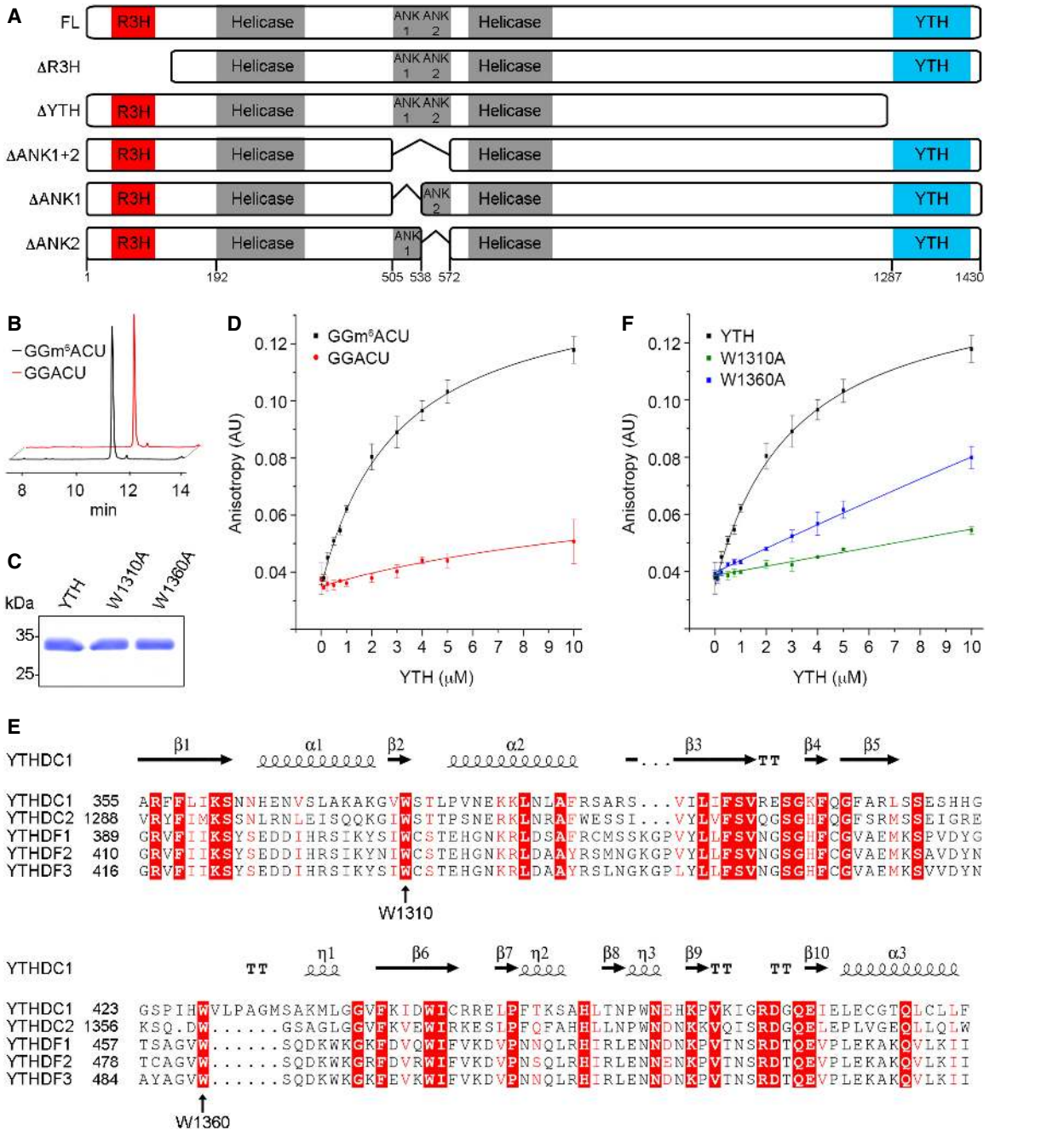

FIGURE 1. The YTH domain of YTHDC2 preferentially binds m^{6}A-containing RNAs. (*A*) Schematic view of the defined domains of YTHDC2 (*top*) and truncations used (*middle*, *bottom*). (FL) Full-length YTHDC2, (YTH) YT521-B homology domain, (R3H) RNA binding domain characterized by an R-(X$_3$)-H motif, (ANK) ankyrin repeat. (*B*) Nine-nucleotide RNAs labeled with 5′-fluorescein were prepared by solid-phase synthesis followed by labeling via click chemistry. Purified RNAs were analyzed by anion exchange HPLC monitored by UV absorbance. (*C*) The wild-type YTH domain of YTHDC2 (YTH) and the YTH domain of YTHDC2 carrying W1310A or W1360A substitutions were expressed in *E. coli* and purified. Purified proteins were separated by SDS-PAGE and visualized by Coomassie staining. (*D*) Anisotropy measurements of a fluorescein-labeled RNA containing either a *N*^{6}-methyladenosine (m^{6}A) or an unmodified adenosine in the presence of different amounts of the YTH domain of YTHDC2. Data from three independent experiments are shown as mean ± standard deviation. (*E*) A sequence alignment of YTH domains of the five human YTH domain-containing proteins is shown. Secondary structural features of the YTH domain of YTHDC1 (PBD 4R3I) are shown *above* the corresponding amino acids. (α) alpha helix, (β) beta sheet, (TT) turn, (η) 3$_{10}$-helix. Amino acids conserved in all YTH domain proteins are highlighted with a red background, and letters denoting amino acids with similar properties are shown in red. The tryptophan residues proposed to contribute to formation of a hydrophobic m^{6}A-binding pocket are indicated. (*F*) Anisotropy measurements of a fluorescein-labeled RNA containing an *N*^{6}-methyladenosine (m^{6}A) with different amounts of the wild-type YTH domain of YTHDC2 (YTH) or the YTH domain in which tryptophan 1310 or tryptophan 1360 were substituted for alanine (W1310A and W1360A, respectively). Data from three independent experiments are shown as mean ± standard deviation.

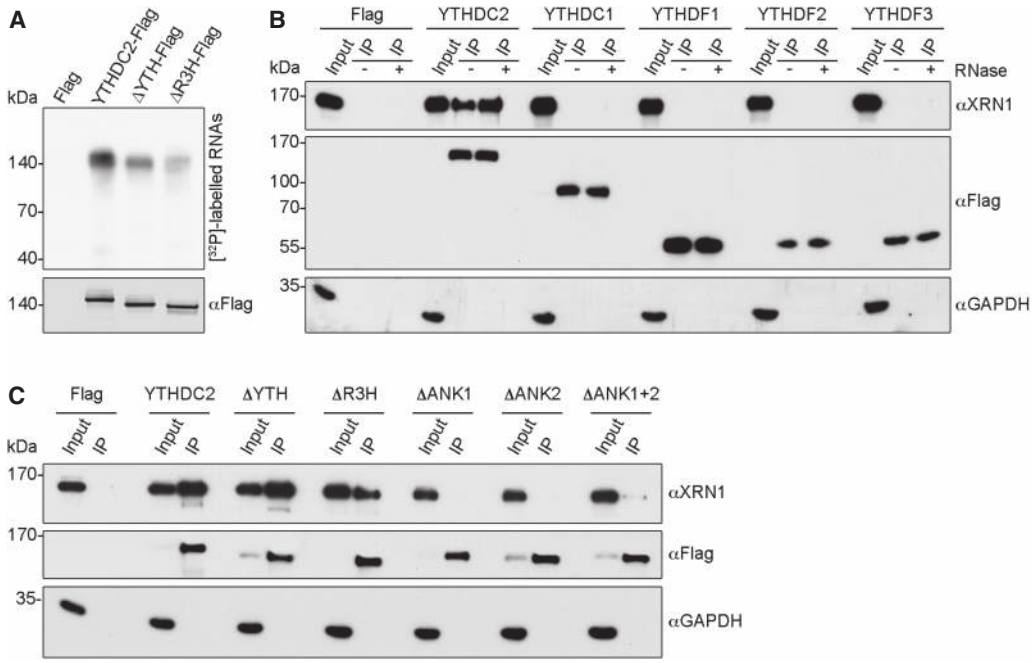

FIGURE 2. Both the YTH and R3H domains contribute to RNA binding by YTHDC2 and YTHDC2 interacts specifically with the 5′–3′ exoribonuclease XRN1 via its ANK repeats. (*A*) Cells expressing equal amounts of Flag-tagged versions of full-length YTHDC2, YTHDC2 lacking the R3H domain (ΔR3H), and YTHDC2 lacking the YTH domain (ΔYTH) were treated with 4-thiouridine and crosslinked in vivo. After tandem affinity purification of crosslinked protein–RNA complexes, RNA trimming and 5′ labeling with [^{32}P], complexes were separated by denaturing PAGE, transferred to a nitrocellulose membrane, and radioactively labeled RNAs were detected using autoradiography. Protein eluates were analyzed by western blotting using an anti-Flag antibody. (*B*) Extracts from HEK293 cells expressing Flag-tagged YTHDC2, YTHDC1, YTHDF1, YTHDF2, YTHDF3, or the Flag tag were used in immunoprecipitation experiments in the presence (+) or absence (–) of RNase A and T1 (RNase). Inputs (1%) and eluates (IP) were analyzed by western blotting using antibodies against XRN1, GAPDH, and the Flag tag. (*C*) Immunoprecipitation experiments were performed and analyzed as in *B* in the absence of RNase treatment using extracts prepared from cells expressing Flag-tagged full-length YTHDC2 (YTHDC2), YTHDC2 lacking the R3H domain (ΔR3H), the YTH domain (ΔYTH), or one or both ankyrin repeats (ΔANK1, ΔANK2, ΔANK1+2). All experiments presented in this figure were performed in duplicate or triplicate and representative data are shown.

considered significant (Supplemental Table 1). Interestingly, aside from the bait, the protein found to be most highly enriched (~7 $\log_2$ fold) with YTHDC2 in both experiments, was the cytoplasmic 5′–3′ exoribonuclease XRN1, suggesting a robust interaction between these proteins and a potential role for YTHDC2 in regulating RNA stability. Notably, a number of ribosomal proteins were also clearly enriched with YTHDC2 implying that YTHDC2 may also associate with ribosomes.

To determine if the interaction observed between YTHDC2 and XRN1 is bridged by RNA and if it is specific for YTHDC2, IP experiments were performed using extracts prepared from cells expressing Flag-tagged YTHDC2, YTHDC1, YTHDF1, YTHDF2, or YTHDF3 or the Flag tag that had either been treated with RNase or left untreated. Analysis of the IP eluates by western blotting using an antibody against XRN1 confirmed the interaction between YTHDC2 and XRN1 and demonstrated that this interaction is still detected after RNase treatment (Fig. 2B), suggesting that it is mediated by protein–protein contacts. Notably, XRN1 was not coprecipitated with the Flag tag or with any of the other YTH domain-containing proteins, implying that its interaction with YTHDC2 is specific (Fig. 2B).

To establish which region(s) of YTHDC2 are required for the interaction of YTHDC2 with XRN1, IP experiments were performed using extracts prepared from cells expressing either the Flag tag or Flag-tagged versions of full-length YTHDC2, ΔR3H, ΔYTH, or YTHDC2 lacking either or both of the ankyrin repeats (ΔANK1, ΔANK2, or ΔANK1+2). Deletion of neither the N-terminal region of YTHDC2 containing the R3H domain nor the C-terminal YTH domain affected the interaction with XRN1 (Fig. 2C). XRN1 was, however, not coprecipitated by YTHDC2 lacking either of the ankyrin repeats (Fig. 2C), demonstrating that the ankyrin repeats of YTHDC2 are essential for this interaction.

YTHDC2 is enriched in perinuclear regions and can associate with ribosomes

To gain insight into the cellular function of YTHDC2, we first analyzed its subcellular localization by performing immunofluorescence using an antibody against endogenous YTHDC2. In addition, the localization of YTHDC2 was analyzed in HEK293 cells expressing YTHDC2-Flag using an anti-Flag antibody. Interestingly, this revealed that in

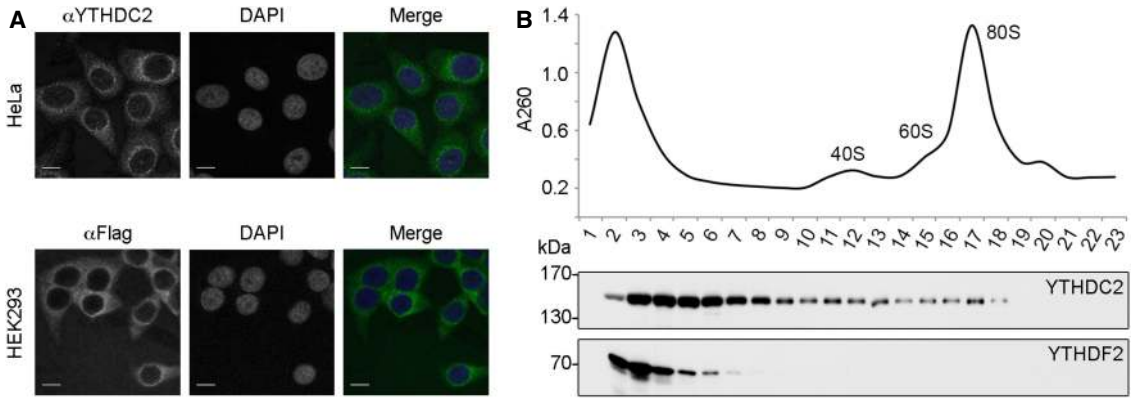

FIGURE 3. YTHDC2 is enriched in perinuclear regions and associates with ribosomes. (*A*) HeLa cells or HEK293 cells expressing Flag-tagged YTHDC2 were fixed, and the localization of YTHDC2 was determined by immunofluorescence using an anti-YTHDC2 antibody (*upper* panels; HeLa cells) or an anti-Flag antibody (*lower* panels; HEK cells). Nuclear material was visualized by DAPI staining and an overlay (merge; YTHDC2, green; DAPI, blue) is shown. Scale bar represents 10 µm. (*B*) Extracts prepared from HeLa cells and a HEK293 cell line expressing FLAG-tagged YTHDF2 were separated by sucrose density gradient centrifugation. The distributions of YTHDC2 and YTHDF2 were determined by western blotting using an anti-YTHDC2 antibody (*upper* panel) or an anti-Flag antibody (*lower* panel; YTHDF2-Flag). The absorbance of the fractions at 260 nm was used to generate a profile on which the peaks corresponding to the 40S and 60S ribosomal subunits and 80S monosomes are indicated. All experiments presented in this figure were performed at least in triplicate and representative data are shown.

both cell lines, the localization of YTHDC2 differs from that of the other YTH domain-containing proteins as although the majority of YTHDC2 is present in the cytoplasm, it is not excluded from nuclei and appears to be enriched in perinuclear regions (Fig. 3A). This finding is consistent with a previous report suggesting that YTHDC2 associates with the endoplasmic reticulum (ER) in HUH-7 and MH-14 cells (Morohashi et al. 2011), but suggests that the protein is also present in other cellular compartments.

The predominantly cytoplasmic localization and perinuclear enrichment of YTHDC2, together with the detection of ribosomal proteins coprecipitated with YTHDC2 (Supplemental Table 1), suggests that a portion of the protein may associate with ribosomes. To determine if YTHDC2 does indeed associate with ribosomes, we performed sucrose density gradient centrifugation of whole cell extracts to separate the small (SSU; 40S) and large (LSU; 60S) ribosomal subunits and 80S monosomes, and then analyzed the distribution of YTHDC2 between fractions containing ribosomal and nonribosomal complexes by western blotting. As a control, this analysis was also performed using an extract prepared from cells expressing Flag-tagged YTHDF2 because this protein has been shown to have ribosome-independent functions in the cytoplasm (Wang et al. 2014). The absorbance of the obtained gradient fractions at 260 nm was used to generate a profile from which the fractions containing the ribosomal subunits and monosomes were identified (Fig. 3B; upper panel). As anticipated, YTHDF2 was exclusively detected in the upper fractions containing free proteins and small, nonribosomal complexes (Fig. 3B; lower panel). Although YTHDC2 was also detected in these fractions, a significant proportion of YTHDC2 co-migrated with 40S complexes and with 80S monosomes (Fig. 3B; middle panel) indicating that YTHDC2 can indeed associate with ribosomes. The finding that only a fraction of YTHDC2 is associated with the ribosome suggests that the interaction of YTHDC2 with the ribosome is likely to be dynamic.

YTHDC2 contacts the head region of the small ribosomal subunit

In humans, the 40S ribosomal subunit contains the 18S rRNA and 33 ribosomal proteins (RPs) and together with multiple translation initiation factors, it mediates scanning of the mRNA to determine the start codon in translation initiation. During translation elongation, the 40S subunit is responsible for decoding of mRNA codons whereas the 60S subunit, which is assembled from the 28S, 5.8S, and 5S rRNAs as well as 47 RPs, contains the peptidyl transferase center that mediates formation of peptide bonds during protein synthesis (Anger et al. 2013). To determine where YTHDC2 contacts the ribosome, we used the crosslinking and analysis of cDNA method (CRAC) (Bohnsack et al. 2012; Sloan et al. 2015; Memet et al. 2017). HEK293 cells expressing YTHDC2-Flag or the Flag tag were grown in the presence of 4-thiouridine and crosslinked using light of 365 nm. Covalently crosslinked protein–RNA complexes were tandem affinity purified and RNAs were subjected to a partial RNase digest to obtain a footprint of YTHDC2 on its associated RNAs. After radiolabeling of RNAs, complexes were separated by polyacrylamide gel electrophoresis, transferred to a nitrocellulose membrane and visualized by autoradiography. Only a single band of

radiolabeled RNAs that migrated at the molecular weight of YTHDC2-Flag was detected and excised (Fig. 4A). RNA fragments bound to YTHDC2 were isolated, ligated to adaptors and used to generate a cDNA library that was subjected to Illumina deep sequencing. The obtained sequence reads were mapped to the human genome and reads containing a specific T–C mutation, arising from nucleotide misincorporation during the reverse transcription step due to the presence of 4-thiouridine in the cellular RNAs, were selected. To identify the ribosome binding site of YTHDC2, the distribution of reads mapping to the rDNA sequence encoding the 47S pre-rRNA transcript consisting of the sequences of three of the mature rRNAs (18S, 5.8S, and 28S rRNAs) flanked by internal and external transcribed spacers, was first examined in several independent experiments. This revealed that, compared to the

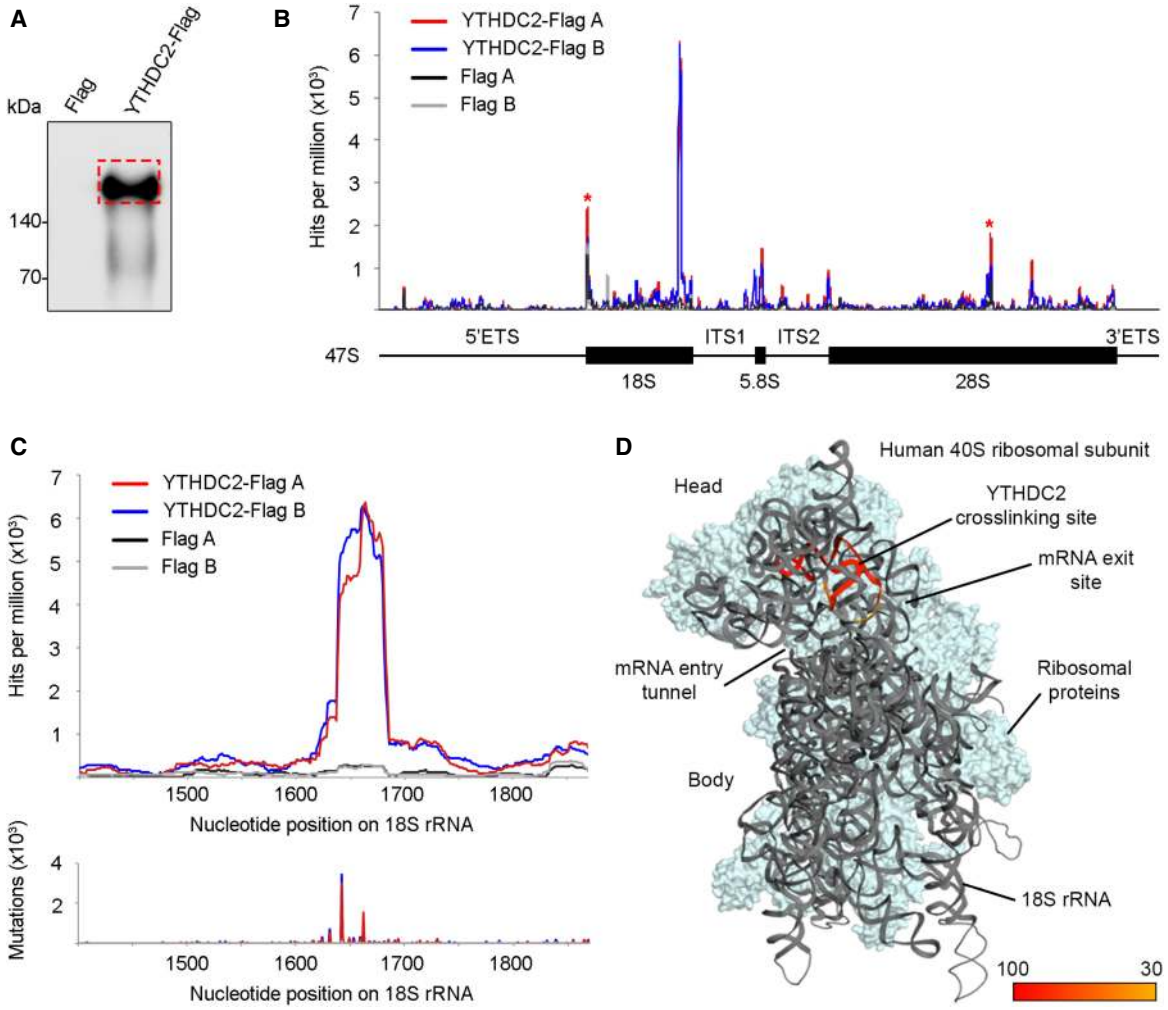

FIGURE 4. YTHDC2 contacts the head region of the small ribosomal subunit. (*A*) HEK293 cells expressing YTHDC2-Flag or the Flag tag were UV crosslinked in vivo. Protein–RNA complexes were tandem affinity purified, and RNAs were trimmed, ligated to adaptors, and labeled at the 5′ end using [^{32}P]. Complexes were separated by PAGE, transferred to a nitrocellulose membrane, and labeled RNAs were visualized by autoradiography. The area excised from the membrane is indicated by red boxes. (*B*) RNA fragments isolated from the membrane shown in *A* were used to prepare a cDNA library that was subjected to Illumina sequencing. The obtained sequence reads were mapped to the human genome, and the number of reads per nucleotide mapped to the rDNA sequence is shown *above* a schematic view of the 47S pre-rRNA transcript containing the sequences of the mature 18S, 5.8S, and 28S rRNAs. (ETS) external transcribed spacer, (ITS) internal transcribed spacer. Asterisks indicate peaks that are present in both YTHDC2-Flag and Flag samples. Three independent CRAC experiments were performed and two representative data sets are presented. (*C*) Magnified views of the YTHDC2-Flag and Flag CRAC reads mapping close to the 3′ end of the 18S rRNA are shown. *Lower* panel indicates the number and position of T–C mutations that are introduced as a result of nucleotide mis-incorporation during reverse transcription at sites where a 4-thiouridine is crosslinked to an amino acid. (*D*) The number of reads in the YTHDC2-Flag A data set mapping to each nucleotide of the 18S rRNA are shown on the 3D structure of the mature 18S rRNA (PDB 4V6X) using a color scale in which the nucleotides to which the maximum number of reads map are shown in red (100%) and nucleotides with lesser numbers of mapped reads are indicated in yellow (above a threshold of 30%). The ribosomal proteins are indicated in pale cyan, the 18S rRNA in gray, and key structural features of the small ribosomal subunit are labeled.

control samples derived from cells expressing the Flag tag, the samples derived from cells expressing YTHDC2-Flag contained a large number of reads that mapped toward the 3′ end of the 18S rRNA (Fig. 4B). Closer inspection of the distribution of reads mapping to the 18S rRNA showed that the majority of reads mapped between nucleotides ~1630 and 1690 (Fig. 4C), suggesting that this sequence is bound by YTHDC2 in vivo. Having established the rRNA sequence contacted by YTHDC2, we next determined the position of this crosslinking site on the mature ribosome by mapping the CRAC data to the available structure of the human 80S ribosome (Anger et al. 2013). The YTHDC2 crosslinking site was found to be in the "head" region of the 40S subunit. While A1832 of the human 18S rRNA is N^6-methylated (Piekna-Przybylska et al. 2008), this site does not lie within the identified YTHDC2 crosslinking site, implying that the crosslinking site does not reflect a contact between the YTH domain of YTHDC2 and this m^{6}A. The YTHDC2 crosslinking site is, however, in close proximity to the mRNA entry tunnel and exit site (Fig. 4D), suggesting that YTHDC2 may regulate the association of m^{6}A-containing mRNAs with the ribosome for translation.

DISCUSSION

Proteins of the YTH domain family have emerged as important regulators of different aspects of gene expression through their ability to recognize and specifically bind to RNAs containing m^{6}As. While YTHDC1 functions in the regulation of pre-mRNA splicing in the nucleus (Xiao et al. 2016), YTHDF1, YTHDF2, and YTHDF3 have been suggested to function cooperatively in the cytoplasm to promote the efficient translation and degradation of specific m^{6}A-containing mRNAs (Wang et al. 2014, 2015; Shi et al. 2017), thereby eliciting rapid alterations in the gene expression profile of cells. The fifth YTH domain-containing protein in human cells, YTHDC2, is unique among the YTH domain proteins as it is present in both the cytoplasm and nucleus, and in addition to its YTH domain, it contains additional RNA binding and protein–protein interaction domains. Our data, together with that of several parallel studies (Bailey et al. 2017; Hsu et al. 2017; Wojtas et al. 2017), suggest that in different cell types YTHDC2 directs specific subsets of mRNAs for rapid expression and degradation. YTHDC2 is highly expressed in testes cells where it was recently shown to bind and regulate the expression and stability of m^{6}A-containing germline transcripts that encode proteins involved in spermatogenesis and that YTHDC2 is therefore important for progression through meiosis (Hsu et al. 2017; Wojtas et al. 2017).

Although YTHDC2 appears to perform similar functions to the YTHDF1-3 proteins in the cytoplasm by promoting interactions between specific mRNAs and the ribosome as well as affecting the stability of its mRNA interaction partners, the mechanisms by which these m^{6}A readers elicit such regulation of mRNAs seem to differ. The common feature of these proteins, namely their binding to m^{6}A-containing mRNAs, is coupled to diverse protein–protein and/or protein–RNA interactions that regulate the fate of the substrate RNAs. YTHDF1 and YTHDF3 have been reported to increase the translation efficiency of their substrate mRNAs by recruitment of translation initiation factors, whereas the binding of YTHDC2 to the 18S rRNA of the small ribosomal subunit in close proximity to the mRNA entry tunnel and exit site suggests that YTHDC2 directly bridges interactions between m^{6}A-containing mRNAs and the ribosome to promote translation. Similarly, both YTHDF2 and YTHDC2 have been suggested to trigger the degradation of their associated transcripts (Wang et al. 2014; Bailey et al. 2017; Hsu et al. 2017; Wojtas et al. 2017). In the case of YTHDF2, its recruitment to m^{6}A-containing mRNAs leads to their relocalization to P-bodies, which are distinct cytoplasmic foci that contain many RNA decay factors. Moreover, YTHDF2 was found to associate with the CCR4-NOT deadenylation complex through an interaction with CNOT1, suggesting that this reader protein promotes rapid mRNA turnover by enhancing the rate of the deadenylation step, thereby making mRNAs more susceptible to RNA decay. Via its ankyrin repeats, YTHDC2 interacts specifically, and in an RNA-independent manner, with the major cytoplasmic 5′–3′ exoribonuclease XRN1. This suggests that, in contrast to YTHDF2, YTHDC2 regulates RNA stability by increasing the local concentration of the RNA degradation machinery at specific mRNA substrates. Why these two m^{6}A reader proteins utilize different mechanisms to promote the degradation of their associated RNAs remains unclear, especially as deadenylation and exonucleolytic processing are closely coupled processes during RNA decay.

It has previously been suggested that the YTH domain of YTHDC2 has weaker affinity for m^{6}A-containing RNAs than the other human YTH domains (Xu et al. 2015). While the YTH domain is required for the interaction of YTHDC2 with cellular RNAs (Fig. 2A) and likely provides the specificity to substrate selection, the observation that the R3H domain also contributes to RNA binding by YTHDC2 in vivo implies that the R3H domain may help stabilize the interactions between YTHDC2 and its m^{6}A-containing substrates. It has recently been reported that YTHDC2 is an active RNA-dependent ATPase (Wojtas et al. 2017), implying that the helicase activity also contributes to its cellular function. It is possible that the remodeling activity of YTHDC2 facilitates access of the YTH domain to m^{6}As on structured mRNA substrates. Alternatively, the helicase domain may regulate the association of YTHDC2 or its substrate mRNAs with the ribosome; remodeling of the head region of the 40S subunit by YTHDC2 may either facilitate access of YTHDC2 substrates to the mRNA entry tunnel or it is possible that the helicase activity of YTHDC2

promotes disassembly of the ribosome–mRNA complex during translation termination to accelerate mRNA decay.

The findings that the YTHDF1-3 proteins and YTHDC2 fast-track both the translation and turnover of specific subsets of mRNAs, raises the question of how these different activities are coordinated. While all five YTH domain proteins preferentially bind m^{6}A-containing RNAs over non-modified RNAs using a similar binding mechanism (Fig. 1 and see for example, Xu et al. 2015), in vivo the YTH domain-containing proteins only bind subsets of m^{6}A-containing mRNAs. This suggests that either elements of the YTH domain outside the m^{6}A-pocket endow specificity for m^{6}A modifications that lie within particular sequence motifs (e.g., Am^{6}AC or Gm^{6}AC) or that other regions of the YTH domain-containing proteins contribute to the recognition of target RNAs. Due to the identification of many common target mRNAs for the YTHDF1-3 proteins, it has been suggested that particular mRNAs can be sequentially bound by different YTH domain-containing proteins such that initial binding by YTHDF1 or YTHDF3 facilitates rapid translation and that subsequent association with YTHDF2 ultimately leads to mRNA turnover. In contrast, the protein and RNA interactions of YTHDC2 suggest that it likely serves to both increase the local concentration of 40S in proximity of specific m^{6}A-containing mRNAs to enhance their translation, as well as enriching XRN1 in the vicinity of translating ribosomes to subsequently promote efficient mRNA turnover. These alternative functions of YTHDC2 must therefore be precisely regulated to enable a single protein to contribute to both aspects of the rapid, but short-lived, mRNA expression response.

MATERIALS AND METHODS

Molecular cloning

The coding sequences of YTHDC2 (NM_022828.4), YTHDC1 (NM_001031732.3), YTHDF1 (NM_017798.3), YTHDF2 (NM_016258.2), or YTHDF3 (NM_152758.5) were cloned into a pcDNA5 vector for expression of the proteins with a C-terminal His_6-Prc (PreScission protease site)-2xFlag (Flag) tag from a tetracycline regulatable promoter in human cells. Similar constructs for the expression of truncated forms of YTHDC2 lacking the R3H domain (ΔR3H; amino acids 192–1430), the YTH domain (ΔYTH; amino acids 1–1287), the ankyrin repeat 1 (ΔANK1; amino acids 1–505 + 539–1430), the ankyrin repeat 2 (ΔANK2; amino acids 1–538 + 572–1430), or both ankyrin repeats (ΔANK1+2; amino acids 1–505 + 572–1430) were also generated. The sequence encoding the YTH domain of YTHDC2 (amino acids 1277–1430) was cloned into a pQE80-derivative vector for the expression of this peptide with an N-terminal His_{10}-ZZ tag from an IPTG-regulatable promoter in *E. coli*. Site-directed mutagenesis was used to generate constructs for the expression of $YTHDC2_{1277–1430}$ in which tryptophan 1310 or 1360 were converted to alanine (W1310A and W1360A) and constructs were verified by sequencing.

Recombinant protein expression, RNA synthesis, and anisotropy measurements

Expression of His_{10}-ZZ-tagged $YTHDC2_{1277–1430}$, or $YTHDC2_{1277–1430}$ carrying W1310A or W1360A substitutions was induced in BL21-Codon Plus cells by addition of 0.3 mM IPTG overnight at 18°C. The cells were then harvested and lysed by sonication in a buffer containing 30 mM Tris-HCl pH 7.4, 150 mM NaCl, 1 mM $MgCl_2$, 10% glycerol, and 1 mM PMSF. After centrifugation at 25,000*g* for 30 min at 4°C, His-tagged proteins in the soluble extract were retrieved on cOmplete His-Tag purification resin (Roche). After washing steps with a buffer containing 30 mM Tris-HCl pH 7.4, 300 mM NaCl, 1 mM $MgCl_2$, 15 mM imidazole, 10% glycerol, proteins were eluted in 30 mM Tris-HCl pH 7.4, 150 mM NaCl, 1 mM $MgCl_2$, 500 mM imidazole, 10% glycerol. Elution fractions containing proteins were pooled and dialyzed against a buffer containing 30 mM Tris-HCl pH 7.4, 120 mM NaCl, 2 mM $MgCl_2$, 20% glycerol. The concentration of the purified proteins was determined using Bradford reagent (Thermo Fisher) and proteins were visualized by SDS-PAGE followed by Coomassie staining.

RNA oligonucleotides (5′-Hex-CCGGACUGU-3′ and 5′-Hex-CCGGm^{6}ACUGU-3′) were prepared by solid-phase synthesis on controlled-pore-glass (CPG) using 5′-*O*-(4,4′-dimethoxytrityl)-2′-*O*-(triisopropylsilyloxymethyl)-protected ribonucleoside phosphoramidites and 5′-hexynyl phosphoramidite. The *N*^{6}-methyladenosine building block was prepared as previously described (Höbartner et al. 2003). After deprotection and purification by denaturing PAGE (20% acrylamide, 7 M urea), the oligonucleotides were labeled with 6-FAM-azide (3 mM) in the presence of CuBr and TBTA (6 mM each) in water/dimethyl sulfoxide/*tert*-butanol (4/3/1) at 37°C for 2 h, followed by precipitation and PAGE purification. The concentration of labeled RNA was determined by UV absorbance at 260 nm, and the identity and homogeneity of fluorescent RNAs was confirmed by ESI-MS (mol. wt. found for m^{6}A-RNA: 3463.3, unmodified RNA: 3449.1) and analytical anion exchange HPLC.

For anisotropy measurements, proteins were re-dialysed against a buffer containing 30 mM Tris-HCl pH 7.5, 120 mM NaCl) overnight. Reactions containing 0–10 µM protein and 20 nM fluorescein-labeled RNAs (5′-Fl-CCGGACUGU-3′ or 5′-Fl-CCGGm^{6}ACUGU-3′) in 30 mM Tris-HCl pH 7.5, 120 mM NaCl were incubated at room temperature (RT) for 5 min. Anisotropy measurements were then performed at 25°C using a FluoroMax-4 spectrofluorometer (Horiba Scientific). The data were analyzed using the following equation:

$$r = r_0 + \frac{\Delta r_{max}}{[RNA]_{tot}} \cdot \left(\frac{[protein]_{tot} + [RNA]_{tot} + K_d}{2} - \sqrt{\left(\frac{[protein]_{tot} + [RNA]_{tot} + K_d}{2} \right)^2 - [protein]_{tot}[RNA]_{tot}} \right),$$

where r_0 is the anisotropy of free RNA, Δr_{max} is the amplitude, and $[protein]_{tot}$ and $[RNA]_{tot}$ are the total protein and total RNA concentrations, respectively.

Human cell culture and generation of stable cell lines

HEK293 and HeLa CCL2 cells were cultured according to standard protocols in 1× Dulbecco's modified Eagle's medium

(DMEM) supplemented with 10% fetal calf serum (FCS) at 37°C with 5% CO_2. Cell lines for the expression of Flag-tagged YTH domain-containing proteins were generated by transfection of the pcDNA5-based constructs into HEK293 Flp-In T-Rex cell (Thermo Fisher Scientific) according to the manufacturer's instructions. Stably transfected cells were selected using hygromycin and blasticidin and expression of the transgene was induced by addition of tetracycline for 24 h before use.

Microscopy

Immunofluorescence was essentially performed as previously described (Warda et al. 2016). In brief, HeLa cells or HEK293 cells expressing YTHDC2-Flag were grown on coverslips and fixed using 4% paraformaldehyde in PBS for 10 min at RT. Cells were permeabilized using 0.1% triton-X-100 in PBS for 15 min before blocking with 10% FCS and 0.1% triton-100 in PBS for 1 h at room temperature. Cells were then incubated with an anti-YTHDC2 antibody (Sigma HPA037364) or an anti-Flag antibody (Sigma F3165) in 10% FCS and PBS for 2 h at room temperature, washed thoroughly and then incubated with a secondary antibody (Alexa Fluor 488-conjugated donkey anti-rabbit; Jackson ImmunoResearch) for a further 2 h. After further washing steps coverslips were mounted using medium containing DAPI (Vectashield; Vector Laboratories). Finally, cells were analyzed by confocal microscopy using a ConfoCor2 microscope (Carl Zeiss).

Immunoprecipitation of complexes and sucrose density gradient analysis

Immunoprecipitation experiments were essentially performed as previously described in Sloan et al. (2015) and Memet et al. (2017). HEK293 stable cell lines were treated with 1 µg/mL tetracycline for 24 h to induce expression of Flag-tagged YTH domain-containing proteins or the Flag tag. Cells were lysed by sonication in a buffer containing 150 mM KCl, 20 mM HEPES pH 8.0, and 0.1 mM DTT, and extracts were supplemented with 0.2 % triton X-100, 10% glycerol, and 1.5 mM $MgCl_2$. After centrifugation to precipitate cell debris, complexes containing Flag-tagged proteins were retrieved on anti-Flag M2 magnetic beads (Sigma Aldrich) either directly or after treatment with 4.5 U/mL RNase A and 1 U/mL RNase T1 for 15 min at room temperature. Bound proteins were eluted by addition of 250 µg/mL FLAG peptide (Sigma Aldrich) at 12°C for 30 min. Proteins were precipitated using 20% trichloroacetic acid (TCA), separated by denaturing polyacrylamide gel electrophoresis and analyzed by mass spectrometry as described in Atanassov and Urlaub (2013). In brief, relevant lanes were excised, fragmented, and proteins were digested with trypsin before nanoLC-MS/MS analysis. Peak lists were extracted from the raw data using Raw2MSMS software, and proteins were identified using MASCOT 2.4 software (Matrixscience) and compared to the UniProtKB human proteome version 2016.01. The log2 fold enrichment of proteins with YTHDC2 was determined by calculating a ratio between the number of spectral counts (unique peptides) identified in the YTHDC2-Flag or Flag-YTHDC2 samples and the control (Flag) sample. To enable such a ratio to be generated for proteins for which no unique peptides were detected in the Flag sample, the number of spectral counts was increased by 1. Alternatively, eluates were analyzed by western blotting using anti-XRN1 (Bethyl A300-443A), anti-Flag (Sigma F3165), and anti-GAPDH (GeneTex GTX627408) antibodies.

For sucrose density gradient centrifugation, HeLa cells or HEK293 cells expressing YTHDF2-Flag were lysed by sonication in a buffer containing 50 mM Tris pH 7.5, 100 mM NaCl, 5 mM $MgCl_2$, and 1 mM DTT. The cleared, whole cell extracts were separated on 10-45% sucrose gradients in an SW-40Ti rotor for 16 h at 23,500 rpm as previously described (Memet et al. 2017). Following centrifugation, gradients were fractionated and the absorbance of each fraction at 260 nm was determined using a NanoDrop (ThermoFisher). Proteins in each fraction were then precipitated using TCA as described above and analyzed by western blotting using antibodies against YTHDC2 (Bethyl A303-026A) or the Flag tag.

Crosslinking and analysis of cDNA (CRAC)

CRAC experiments were essentially performed as previously described (Bohnsack et al. 2012; Haag et al. 2015; Sloan et al. 2015; Memet et al. 2017). In brief, HEK293 cells expressing Flag-tagged YTHDC2, truncated versions of YTHDC2 or the Flag tag were grown in the presence of 100 µM 4-thiouridine for 6 h prior to crosslinking at 365 nm in a Stratalinker (Agilent). Cells were harvested and protein–RNA complexes were isolated by tandem affinity purification on anti-Flag magnetic beads (native conditions) and on NiNTA resin (denaturing conditions). Partial RNase digestion was performed, and coprecipitated RNAs were 5′-end labeled with ^{32}P and ligated to sequencing adaptors. Protein–RNA complexes were separated by polyacrylamide gel electrophoresis, transferred to a nitrocellulose membrane and visualized by autoradiography. Areas of the membrane containing specific signals were excised and RNAs were isolated. After reverse transcription and PCR amplification, the cDNA library was subjected to Illumina sequencing. The obtained sequence reads were mapped to the human genome (GRCh37.p13) as previously described (Haag et al. 2017). The number of reads mapping to each nucleotide of the rDNA sequence coding for the 47S pre-rRNA were modeled onto the cryo-electron microscopy structure of the human 80S ribosome (PBD 4V6X) (Anger et al. 2013) using python scripts.

SUPPLEMENTAL MATERIAL

Supplemental material is available for this article.

ACKNOWLEDGMENTS

We thank Henning Urlaub and Uwe Plessmann for mass spectrometry analysis. This work was supported by the Deutsche Forschungsgemeinschaft (SPP1784: BO 3442/2-2 to M.T.B.; HO4436/2-2 to C.H.) and the University Medical Center Göttingen (to M.T.B.).

Received September 27, 2017; accepted June 26, 2018.

REFERENCES

Adams JM, Cory S. 1975. Modified nucleosides and bizarre 5′-termini in mouse myeloma mRNA. *Nature* **255:** 28–33.

Alarcón CR, Goodarzi H, Lee H, Liu X, Tavazoie S, Tavazoie SF. 2015. HNRNPA2B1 is a mediator of m^{6}A-dependent nuclear RNA processing events. *Cell* **162:** 1299–1308.

Anger AM, Armache JP, Berninghausen O, Habeck M, Subklewe M, Wilson DN, Beckmann R. 2013. Structures of the human and *Drosophila* 80S ribosome. *Nature* **497:** 80–85.

Atanassov I, Urlaub H. 2013. Increased proteome coverage by combining PAGE and peptide isoelectric focusing: comparative study of gel-based separation approaches. *Proteomics* **13:** 2947–2955.

Bailey AS, Batista PJ, Gold RS, Chen YG, de Rooij DG, Chang HY, Fuller MT. 2017. The conserved RNA helicase YTHDC2 regulates the transition from proliferation to differentiation in the germline. *Elife* **6:** e26116.

Bartosovic M, Molares HC, Gregorova P, Hrossova D, Kudla G, Vanacova S. 2017. *N*^{6}-methyladenosine demethylase FTO targets pre-mRNAs and regulates alternative splicing and 3′-end processing. *Nucleic Acids Res* **45:** 11356–11370.

Bohnsack MT, Tollervey D, Granneman S. 2012. Identification of RNA helicase target sites by UV cross-linking and analysis of cDNA. *Methods Enzymol* **511:** 275–288.

Chen K, Lu Z, Wang X, Fu Y, Luo GZ, Liu N, Han D, Dominissini D, Dai Q, Pan T, et al. 2015. High-resolution *N*^{6}-methyladenosine (m^{6}A) map using photo-crosslinking-assisted m^{6}A sequencing. *Angew Chem Int Ed Engl* **54:** 1587–1590.

Choi J, Ieong KW, Demirci H, Chen J, Petrov A, Prabhakar A, O'Leary SE, Dominissini D, Rechavi G, Soltis SM, et al. 2016. *N*^{6}-methyladenosine in mRNA disrupts tRNA selection and translation-elongation dynamics. *Nat Struct Mol Biol* **23:** 110–115.

Cui Q, Shi H, Ye P, Li L, Qu Q, Sun G, Sun G, Lu Z, Huang Y, Yang CG, et al. 2017. m^{6}A RNA methylation regulates the self-renewal and tumorigenesis of glioblastoma stem cells. *Cell Rep* **18:** 2622–2634.

Dai X, Wang T, Gonzalez G, Wang Y. 2018. Identification of YTH domain-containing proteins as the readers for *N*1-methyladenosine in RNA. *Anal Chem* **90:** 6380–6384.

Desrosiers R, Friderici K, Rottman F. 1974. Identification of methylated nucleosides in messenger RNA from Novikoff hepatoma cells. *Proc Natl Acad Sci* **71:** 3971–3975.

Dominissini D, Moshitch-Moshkovitz S, Schwartz S, Salmon-Divon M, Ungar L, Osenberg S, Cesarkas K, Jacob-Hirsch J, Amariglio N, Kupiec M, et al. 2012. Topology of the human and mouse m^{6}A RNA methylomes revealed by m^{6}A-seq. *Nature* **485:** 201–206.

Du H, Zhao Y, He J, Zhang Y, Xi H, Liu M, Ma J, Wu L. 2016. YTHDF2 destabilizes m^{6}A-containing RNA through direct recruitment of the CCR4-NOT deadenylase complex. *Nat Commun* **7:** 12626.

Dubin DT, Taylor RH. 1975. The methylation state of poly A-containing messenger RNA from cultured hamster cells. *Nucleic Acids Res* **2:** 1653–1668.

Haag S, Warda AS, Kretschmer J, Günnigmann MA, Höbartner C, Bohnsack MT. 2015. NSUN6 is a human RNA methyltransferase that catalyzes formation of m^{5}C72 in specific tRNAs. *RNA* **21:** 1532–1543.

Haag S, Kretschmer J, Sloan KE, Bohnsack MT. 2017. Crosslinking methods to identify RNA methyltransferase targets in vivo. *Methods Mol Biol* **1562:** 269–281.

Höbartner C, Kreutz C, Flecker E, Ottenschläger E, Pils W, Grubmayr K, Micura R. 2003. The synthesis of 2′-O -[(triisopropylsilyl)oxy]methyl (TOM) phosphoramidites of methylated ribonucleosides (m^{1}G, m^{2}G, m$^2{}_2$G, m^{1}I, m^{3}U, m^{4}C, m^{6}A, m$^6{}_2$A) for use in automated RNA solid-phase synthesis. *Chem Mon* **134:** 851–873.

Hsu PJ, Zhu Y, Ma H, Guo Y, Shi X, Liu Y, Qi M, Lu Z, Shi H, Wang J, et al. 2017. Ythdc2 is an *N*^{6}-methyladenosine binding protein that regulates mammalian spermatogenesis. *Cell Res* **27:** 1115–1127.

Huang H, Weng H, Sun W, Qin X, Shi H, Wu H, Zhao BS, Mesquita A, Liu C, Yuan CL, et al. 2018. Recognition of RNA *N*^{6}-methyladenosine by IGF2BP proteins enhances mRNA stability and translation. *Nat Cell Biol* **20:** 285–295.

Jia G, Fu Y, Zhao X, Dai Q, Zheng G, Yang Y, Yi C, Lindahl T, Pan T, Yang YG, et al. 2011 *N*^{6}-methyladenosine in nuclear RNA is a major substrate of the obesity-associated FTO. *Nat Chem Biol* **7:** 885–887.

Kasowitz SD, Ma J, Anderson SJ, Leu NA, Xu Y, Gregory BD, Schultz RM, Wang PJ. 2018. Nuclear m^{6}A reader YTHDC1 regulates alternative polyadenylation and splicing during mouse oocyte development. *PLoS Genet* **14:** e1007412.

Ke S, Alemu EA, Mertens C, Gantman EC, Fak JJ, Mele A, Haripal B, Zucker-Scharff I, Moore MJ, Park CY, et al. 2015. A majority of m^{6}A residues are in the last exons, allowing the potential for 3′ UTR regulation. *Genes Dev* **29:** 2037–2053.

Ke S, Pandya-Jones A, Saito Y, Fak JJ, Vågbø CB, Geula S, Hanna JH, Black DL, Darnell JEJr, Darnell RB. 2017. m^{6}A mRNA modifications are deposited in nascent pre-mRNA and are not required for splicing but do specify cytoplasmic turnover. *Genes Dev* **31:** 990–1006.

Lence T, Akhtar J, Bayer M, Schmid K, Spindler L, Ho CH, Kreim N, Andrade-Navarro MA, Poeck B, Helm M, et al. 2016. m^{6}A modulates neuronal functions and sex determination in *Drosophila*. *Nature* **540:** 242–247.

Lin S, Choe J, Du P, Triboulet R, Gregory RI. 2016. The m^{6}A methyltransferase METTL3 promotes translation in human cancer cells. *Mol Cell* **62:** 335–345.

Linder B, Grozhik AV, Olarerin-George AO, Meydan C, Mason CE, Jaffrey SR. 2015. Single-nucleotide-resolution mapping of m^{6}A and m^{6}Am throughout the transcriptome. *Nat Methods* **12:** 767–772.

Liu J, Yue Y, Han D, Wang X, Fu Y, Zhang L, Jia G, Yu M, Lu Z, Deng X, et al. 2014. A METTL3-METTL14 complex mediates mammalian nuclear RNA *N*^{6}-adenosine methylation. *Nat Chem Biol* **10:** 93–95.

Liu N, Dai Q, Zheng G, He C, Parisien M, Pan T. 2015. *N*^{6}-methyladenosine-dependent RNA structural switches regulate RNA-protein interactions. *Nature* **518:** 560–564.

Mauer J, Luo X, Blanjoie A, Jiao X, Grozhik AV, Patil DP, Linder B, Pickering BF, Vasseur JJ, Chen Q, et al. 2017. Reversible methylation of m^{6}Am in the 5′ cap controls mRNA stability. *Nature* **541:** 371–375.

Memet I, Doebele C, Sloan KE, Bohnsack MT. 2017. The G-patch protein NF-κB-repressing factor mediates the recruitment of the exonuclease XRN2 and activation of the RNA helicase DHX15 in human ribosome biogenesis. *Nucleic Acids Res* **45:** 5359–5374.

Meyer KD, Jaffrey SR. 2017. Rethinking m^{6}A readers, writers, and erasers. *Annu Rev Cell Dev Biol* **33:** 319–342.

Meyer KD, Saletore Y, Zumbo P, Elemento O, Mason CE, Jaffrey SR. 2012. Comprehensive analysis of mRNA methylation reveals enrichment in 3′ UTRs and near stop codons. *Cell* **149:** 1635–1646.

Molinie B, Wang J, Lim KS, Hillebrand R, Lu ZX, Van Wittenberghe N, Howard BD, Daneshvar K, Mullen AC, Dedon P, et al. 2016. m^{6}A-LAIC-seq reveals the census and complexity of the m^{6}A epitranscriptome. *Nat Methods* **13:** 692–698.

Morohashi K, Sahara H, Watashi K, Iwabata K, Sunoki T, Kuramochi K, Takakusagi K, Miyashita H, Sato N, Tanabe A, et al. 2011. Cyclosporin A associated helicase-like protein facilitates the association of hepatitis C virus RNA polymerase with its cellular cyclophilin B. *PLoS One* **6:** e18285.

Patil DP, Chen CK, Pickering BF, Chow A, Jackson C, Guttman M, Jaffrey SR. 2016. m^{6}A RNA methylation promotes XIST-mediated transcriptional repression. *Nature* **537:** 369–373.

Pendleton KE, Chen B, Liu K, Hunter OV, Xie Y, Tu BP, Conrad NK. 2017. The U6 snRNA m^{6}A methyltransferase METTL16 regulates SAM synthetase intron retention. *Cell* **169:** 824–835.

Piekna-Przybylska D, Decatur WA, Fournier MJ. 2008. The 3D rRNA modification maps database: with interactive tools for ribosome analysis. *Nucleic Acids Res* **36:** D178–D183.

Ping XL, Sun BF, Wang L, Xiao W, Yang X, Wang WJ, Adhikari S, Shi Y, Lv Y, Chen YS, et al. 2014. Mammalian WTAP is a regulatory subunit of the RNA N^6-methyladenosine methyltransferase. *Cell Res* **24:** 177–189.

Robert X, Gouet P. 2014. Deciphering key features in protein structures with the new ENDscript server. *Nucleic Acids Res* **42:** 320–324.

Roost C, Lynch SR, Batista PJ, Qu K, Chang HY, Kool ET. 2015. Structure and thermodynamics of N^6-methyladenosine in RNA: a spring-loaded base modification. *J Am Chem Soc* **137:** 2107–2115.

Roundtree IA, Evans ME, Pan T, He C. 2017a. Dynamic RNA modifications in gene expression regulation. *Cell* **169:** 1187–1200.

Roundtree IA, Luo GZ, Zhang Z, Wang X, Zhou T, Cui Y, Sha J, Huang X, Guerrero L, Xie P, et al. 2017b. YTHDC1 mediates nuclear export of N^6-methyladenosine methylated mRNAs. *Elife* **6:** e31311.

Schwartz S, Agarwala SD, Mumbach MR, Jovanovic M, Mertins P, Shishkin A, Tabach Y, Mikkelsen TS, Satija R, Ruvkun G, et al. 2013. High-resolution mapping reveals a conserved, widespread, dynamic mRNA methylation program in yeast meiosis. *Cell* **155:** 1409–1421.

Schwartz S, Mumbach MR, Jovanovic M, Wang T, Maciag K, Bushkin GG, Mertins P, Ter-Ovanesyan D, Habib N, Cacchiarelli D, et al. 2014. Perturbation of m^{6}A writers reveals two distinct classes of mRNA methylation at internal and 5′ sites. *Cell Rep* **8:** 284–296.

Shi H, Wang X, Lu Z, Zhao BS, Ma H, Hsu PJ, Liu C, He C. 2017. YTHDF3 facilitates translation and decay of N^6-methyladenosine-modified RNA. *Cell Res* **27:** 315–328.

Sloan KE, Leisegang MS, Doebele C, Ramírez AS, Simm S, Safferthal C, Kretschmer J, Schorge T, Markoutsa S, Haag S, et al. 2015. The association of late-acting snoRNPs with human pre-ribosomal complexes requires the RNA helicase DDX21. *Nucleic Acids Res* **43:** 553–564.

Theler D, Dominguez C, Blatter M, Boudet J, Allain FH. 2014. Solution structure of the YTH domain in complex with N^6-methyladenosine RNA: a reader of methylated RNA. *Nucleic Acids Res* **42:** 13911–13919.

Wang X, He C. 2014. Reading RNA methylation codes through methyl-specific binding proteins. *RNA Biol* **11:** 669–672.

Wang X, Lu Z, Gomez A, Hon GC, Yue Y, Han D, Fu Y, Parisien M, Dai Q, Jia G, et al. 2014. N^6-methyladenosine-dependent regulation of messenger RNA stability. *Nature* **505:** 117–120.

Wang X, Zhao BS, Roundtree IA, Lu Z, Han D, Ma H, Weng X, Chen K, Shi H, He C. 2015. N^6-methyladenosine modulates messenger RNA translation efficiency. *Cell* **161:** 1388–1399.

Wang P, Doxtader KA, Nam Y. 2016a. Structural basis for cooperative function of Mettl3 and Mettl14 methyltransferases. *Mol Cell* **63:** 306–317.

Wang X, Feng J, Xue Y, Guan Z, Zhang D, Liu Z, Gong Z, Wang Q, Huang J, Tang C, et al. 2016b. Structural basis of N^6-adenosine methylation by the METTL3-METTL14 complex. *Nature* **534:** 575–578.

Warda AS, Freytag B, Haag S, Sloan KE, Görlich D, Bohnsack MT. 2016. Effects of the Bowen-Conradi syndrome mutation in EMG1 on its nuclear import, stability and nucleolar recruitment. *Hum Mol Genet* **25:** 5353–5364.

Warda AS, Kretschmer J, Hackert P, Lenz C, Urlaub H, Höbartner C, Sloan KE, Bohnsack MT. 2017. Human METTL16 is a N^6-methyladenosine (m^{6}A) methyltransferase that targets pre-mRNAs and various non-coding RNAs. *EMBO Rep* **18:** 2004–2014.

Wojtas MN, Pandey RR, Mendel M, Homolka D, Sachidanandam R, Pillai RS. 2017. Regulation of m^{6}A Transcripts by the 3′→5′ RNA helicase YTHDC2 Is essential for a successful meiotic program in the mammalian germline. *Mol Cell* **68:** 374–387.

Xiao W, Adhikari S, Dahal U, Chen YS, Hao YJ, Sun BF, Sun HY, Li A, Ping XL, Lai WY, et al. 2016. Nuclear m^{6}A reader YTHDC1 regulates mRNA splicing. *Mol Cell* **61:** 507–519.

Xu C, Wang X, Liu K, Roundtree IA, Tempel W, Li Y, Lu Z, He C, Min J. 2014. Structural basis for selective binding of m^{6}A RNA by the YTHDC1 YTH domain. *Nat Chem Biol* **10:** 927–929.

Xu C, Liu K, Ahmed H, Loppnau P, Schapira M, Min J. 2015. Structural basis for the discriminative recognition of N^6-methyladenosine RNA by the human YT521-B homology domain family of proteins. *J Biol Chem* **290:** 24902–24913.

Xu K, Yang Y, Feng GH, Sun BF, Chen JQ, Li YF, Chen YS, Zhang XX, Wang CX, Jiang LY, et al. 2017. Mettl3-mediated m^{6}A regulates spermatogonial differentiation and meiosis initiation. *Cell Res* **27:** 1100–1114.

Xuan JJ, Sun WJ, Lin PH, Zhou KR, Liu S, Zheng LL, Qu LH, Yang JH. 2017. RMBase v2.0: deciphering the map of RNA modifications from epitranscriptome sequencing data. *Nucleic Acids Res* **46:** D327–334.

Yu J, Chen M, Huang H, Zhu J, Song H, Zhu J, Park J, Ji SJ. 2018. Dynamic m^{6}A modification regulates local translation of mRNA in axons. *Nucleic Acids Res* **46:** 1412–1423.

Zhang Z, Theler D, Kaminska KH, Hiller M, de la Grange P, Pudimat R, Rafalska I, Heinrich B, Bujnicki JM, Allain FH, et al. 2010. The YTH domain is a novel RNA binding domain. *J Biol Chem* **285:** 14701–14710.

Zhao BS, Wang X, Beadell AV, Lu Z, Shi H, Kuuspalu A, Ho RK, He C. 2017a. m^{6}A-dependent maternal mRNA clearance facilitates zebrafish maternal-to-zygotic transition. *Nature* **542:** 475–478.

Zhao BS, Roundtree IA, He C. 2017b. Post-transcriptional gene regulation by mRNA modifications. *Nat Rev Mol Cell Biol* **18:** 31–42.

Zheng G, Dahl JA, Niu Y, Fedorcsak P, Huang CM, Li CJ, Vågbø CB, Shi Y, Wang WL, Song SH, et al. 2013. ALKBH5 is a mammalian RNA demethylase that impacts RNA metabolism and mouse fertility. *Mol Cell* **49:** 18–29.

Zhou J, Wan J, Gao X, Zhang X, Jaffrey SR, Qian SB. 2015. Dynamic m^{6}A mRNA methylation directs translational control of heat shock response. *Nature* **526:** 591–594.

The m^{6}A reader protein YTHDC2 interacts with the small ribosomal subunit and the 5′–3′ exoribonuclease XRN1

Jens Kretschmer, Harita Rao, Philipp Hackert, et al.

RNA 2018 24: 1339-1350 originally published online July 3, 2018
Access the most recent version at doi:10.1261/rna.064238.117